Grain size-sensitive viscoelastic relaxation and seismic properties of polycrystalline MgO

Barnhoorn, A.; Jackson, I.; Fitz Gerald, J. D.; Kishimoto, A.; Itatani, K.

DOI
10.1002/2016JB013126

Publication date
2016

Document Version
Final published version

Published in
JGR Solid Earth

AGU PUBLICATIONS

JGR

Journal of Geophysical Research: Solid Earth

RESEARCH ARTICLE

10.1002/2016JB013126

Key Points:
- High-temperature viscoelastic relaxation in polycrystalline MgO has been quantified
- Shear modulus and dissipation are broadly consistent with the theory of grain boundary sliding
- Extrapolation suggests that ferropericlase might contribute to attenuation in the lower mantle

Correspondence to:
I. Jackson,
ian.jackson@anu.edu.au

Citation:
Barnhoorn, A., I. Jackson, J. D. Fitz Gerald, A. Kishimoto, and K. Itatani (2016), Grain size-sensitive viscoelastic relaxation and seismic properties of polycrystalline MgO, *J. Geophys. Res. Solid Earth*, *121*, 4955–4976, doi:10.1002/2016JB013126.

Received 25 APR 2016
Accepted 13 JUN 2016
Accepted article online 24 JUN 2016
Published online 13 JUL 2016

Grain size-sensitive viscoelastic relaxation and seismic properties of polycrystalline MgO

A. Barnhoorn[1,2], I. Jackson[1], J. D. Fitz Gerald[1], A. Kishimoto[3], and K. Itatani[4]

[1]Research School of Earth Sciences, Australian National University, Canberra, ACT, Australia, [2]Department of Geoscience and Engineering, Faculty of Civil Engineering and Geosciences, Delft University of Technology, Delft, Netherlands, [3]Department of Applied Chemistry, Faculty of Engineering, Okayama University, Okayama, Japan, [4]Department of Materials and Life Sciences, Faculty of Science and Technology, Sophia University, Tokyo, Japan

Abstract Torsional forced-oscillation experiments on a suite of synthetic MgO polycrystals, of high-purity and average grain sizes of 1–100 μm, reveal strongly viscoelastic behavior at temperatures of 800–1300°C and periods between 1 and 1000 s. The measured shear modulus and associated strain energy dissipation both display monotonic variations with oscillation period, temperature, and grain size. The data for the specimens of intermediate grain size have been fitted to a generalized Burgers creep function model that is also broadly consistent with the results for the most coarse-grained specimen. The mild grain size sensitivity for the relaxation time τ_L, defining the lower end of the anelastic absorption band, is consistent with the onset of elastically accommodated grain boundary sliding. The upper end of the anelastic absorption band, evident in the highest-temperature data for one specimen only, is associated with the Maxwell relaxation time τ_M marking the transition toward viscous behavior, conventionally ascribed a stronger grain size sensitivity. Similarly pronounced viscoelastic behavior was observed in complementary torsional microcreep tests, which confirm that the nonelastic strains are mainly recoverable, i.e., anelastic. With an estimated activation volume for the viscoelastic relaxation, the experimentally constrained Burgers model has been extrapolated to the conditions of pressure and temperature prevailing in the Earth's uppermost lower mantle. For a plausible grain size of 10 mm, the predicted dissipation Q^{-1} ranges from ~10^{-3} to ~10^{-2} for periods of 3–3000 s. Broad consistency with seismological observations suggests that the lower mantle ferropericlase phase might account for much of its observed attenuation.

1. Introduction

1.1. Seismological Observations

High-temperature viscoelastic relaxation of the rocks and minerals of the Earth's deep interior is responsible for the attenuation and associated dispersion of seismic shear waves. Such departures from perfectly elastic behavior are most pronounced in the asthenosphere of the upper mantle and in the inner core, in each of which regions maximum dissipation (Q^{-1}) values of order 10^{-2} are inferred, whereas lower values near 0.003 are found for the lower mantle [e.g., *Romanowicz and Mitchell*, 2015]. In the largely crystalline materials of the Earth's mantle, such relaxation is likely to involve both the stress-induced migration of dislocations within individual mineral grains and also sliding on grain and interphase boundaries. Such processes may be enhanced in parts of the Earth's mantle by the presence of trace concentrations of hydrous defects and/or of a small melt fraction [e.g., *Jackson*, 2015].

1.2. Viscoelastic Relaxation by Grain Boundary Sliding: Theory

Grain boundary sliding is commonly invoked to explain the transition from elastic through anelastic to viscous behavior observed in laboratory experiments on fine-grained polycrystalline materials. The theory of grain boundary sliding, dating from the classic work of *Raj and Ashby* [1972], and relevant experimental evidence from silicate and analogue materials has recently been reviewed [*Jackson et al.*, 2014; *Takei et al.*, 2014; *Jackson*, 2015] so that a brief summary will suffice here. The key concept is that of a narrow grain boundary region, distinguished from the crystalline lattices of the neighboring grains by a higher degree of positional disorder and chemical complexity. Accordingly, this boundary region is expected to have generally higher diffusivities for the various atomic and molecular species than the adjacent crystals and hence lower effective viscosity.

It is accordingly envisaged that an increase of temperature and/or timescale of stress application, beyond an appropriate threshold, will result in relative tangential motion (sliding) between adjacent crystals, facilitated by the low boundary viscosity. In the presence of boundary topography, such sliding gives rise to a distribution of normal stresses that cause an accommodating elastic distortion of the neighboring grains and also provide the restoring force for return to the unstrained condition on removal of the applied stress. That the finite amount of additional, nonelastic, strain is fully recoverable means that elastically accommodated grain boundary sliding qualifies as an anelastic relaxation process [*Nowick and Berry*, 1972]. The characteristic timescale τ_e for relaxation by elastically accommodated grain boundary sliding is given by the expression [e.g., *Kê*, 1947; *Nowick and Berry*, 1972]

$$\tau_e = \eta_{gb} d / G_U \delta = \eta_{gb} / G_U \alpha_b. \quad (1)$$

The grain boundary region, of thickness δ and length in the sliding direction comparable with the grain size d (and hence of aspect ratio $\alpha_b = \delta/d$), is assumed to respond to applied stress as a Newtonian fluid, in which the shear stress is the product of strain rate and a viscosity $\eta_{gb} << \eta_{ss}$, the viscosity associated with steady state diffusional creep of the polycrystal. Under conditions of sinusoidally time-varying shear stress, a dissipation peak and associated partial relaxation of the shear modulus (from the unrelaxed value G_U) are expected for an angular frequency $\omega \sim 1/\tau_e$.

At higher temperatures and/or longer timescales of stress application, the distribution of boundary-normal stress is modified by diffusional transport of matter along the grain boundary, ultimately allowing the transition from anelastic toward viscous behavior. The time constant τ_d for the evolution of the distribution of normal stress from that prevailing on completion of elastically accommodated sliding to that associated with steady state diffusional creep, and thus the duration of transient diffusional creep, was identified [*Raj*, 1975; *Gribb and Cooper*, 1998], within a dimensionless multiplicative factor, to be the Maxwell time for diffusional creep with the steady state viscosity η_{ss}, i.e.,

$$\tau_d = (1-\nu) k T d^3 / \left(40\pi^3 G_U \delta D_{gb} \Omega\right) = \eta_{ss} / G_U \quad (2)$$

where ν, k, T, D_{gb}, and Ω are, respectively, the Poisson's ratio, the Boltzmann constant, the absolute temperature, the grain boundary diffusivity, and the molecular volume of the diffusing species. For harmonic loading, such anelastic behavior results in a weakly frequency-/period-dependent dissipation and associated modulus relaxation, of the type often referred to as high-temperature background [e.g., *Nowick and Berry*, 1972].

The classic Raj-Ashby model of grain boundary sliding has recently been revisited by *Morris and Jackson* [2009]. The boundary value problem describing sliding on a fixed periodic piecewise linear interface between two elastic grains, including both low effective viscosity of the grain boundary region and grain boundary diffusion, was solved in the limit of infinitesimal boundary slope for the complete mechanical relaxation spectrum. A dissipation peak located at $\omega \sim 1/\tau_e$ and the diffusionally accommodated sliding regime with $Q^{-1} \sim (\omega\tau_d)^{-1}$ for $\omega < 1/\tau_d$ are separated by a diffusionally assisted sliding regime within which Q^{-1} varies very mildly with frequency. The term "diffusionally assisted" is used to convey the idea that within this regime, diffusion occurs on progressively greater spatial scales (ultimately comparable with the grain size d) with decreasing frequency toward $1/\tau_d$. The width (in frequency or timescale of stress application) of this diffusionally assisted regime is determined by ratio $M = \tau_e/\tau_d$, which is poorly constrained a priori, but inferred from experimental data for fine-grained polycrystals to be $<< 1$ [*Morris and Jackson*, 2009].

Subsequently, a combination of analytical and numerical (finite element) methods has been used to extend the work of *Morris and Jackson* [2009] to finite slopes of the same piecewise linear boundary between elastic grains [*Lee and Morris*, 2010; *Lee et al.*, 2011]. This work, reviewed by *Jackson et al.* [2014], confirms that the qualitative features predicted by the infinitesimal-slope analysis of *Raj and Ashby* [1972] and *Morris and Jackson* [2009] survive when the interface has finite slope, but the overall level of dissipation, which depends strongly on boundary slope, is greatly reduced.

Such micromechanical models of grain boundary sliding thus clearly predict that the first significant indication, with increasing temperature, of the breakdown of strictly elastic behavior in fine-grained materials should be a broad dissipation peak with amplitude of order 10^{-2} and associated modulus dispersion, reflecting anelastic behavior associated with elastically accommodated grain boundary sliding. With further increase in period and/or temperature, diffusion will become progressively more influential. This results first

in additional anelastic strain within a broad diffusionally assisted sliding regime (involving a power law dependence of dissipation upon normalized frequency, i.e., $Q^{-1} \sim (\omega\tau_d)^{-\alpha}$, with $\alpha \sim 0.3$ for the saw-tooth boundary of a two-dimensional array of regular hexagons). For still longer periods/lower frequencies or higher temperatures, the irrecoverable viscous strain of diffusionally accommodated grain boundary sliding will be realized.

1.3. Viscoelastic Relaxation by Grain Boundary Sliding: Observations

The growing body of torsional forced-oscillation data for polycrystalline olivine provides some evidence of a broad dissipation plateau at $\log Q^{-1} \sim -2$ for periods of 1–1000 s and temperatures of ~800°C. This Q^{-1} plateau has been interpreted as the superposition of a dissipation peak of amplitude $\sim 10^{-2}$ upon the usual monotonically frequency (and temperature) dependent high-temperature background. Broadly similar observations of background behavior [*McCarthy et al.*, 2011] and a superimposed dissipation peak have recently been made for borneol, an organic silicate analogue [*Takei et al.*, 2014]. In accord with the predictions of the micromechanical models, both the dissipation peak/plateau and an associated modulus deficit have tentatively been attributed to elastically accommodated grain boundary sliding [*Jackson and Faul*, 2010; *Takei et al.*, 2014; *Jackson et al.*, 2014].

Seismologically observed levels of dissipation (rarely exceeding 0.01) indicate that conditions depart only marginally from ideal elastic behavior. Accordingly, it is the transition from elastic to anelastic behavior that is most relevant to the interpretation of seismological observations. Definitive evidence for or against the occurrence of elastically accommodated grain boundary sliding and of the grain size sensitivity of anelastic relaxation is therefore vital. The present study is an attempt to shed light on grain boundary sliding as a viscoelastic relaxation mechanism through a systematic study of grain size-sensitive behavior of polycrystalline magnesium oxide. MgO is an end-member of the important lower mantle mineral, ferropericlase (or magnesiowüstite). Moreover, its cubic symmetry and associated isotropic thermal expansion mean that even medium to coarse-grained polycrystals can be subjected to large excursions in temperature during mechanical testing without thermal cracking. The opportunity therefore exists to make experimental observations of viscoelastic behavior across an unusually wide range of grain size.

2. Experimental Procedure and Methods for Data Analysis

2.1. Fabrication of Dense Polycrystals of Controlled Grain Size

High-purity MgO powder (>99.99 wt % MgO) with a grain size of 45–60 nm (supplied by Ube Materials Industries Ltd.) has been used for production of high-density cylindrical polycrystalline aggregates (Figures 1 and 2). A multistage procedure of cold isostatic pressing and hot isostatic pressing of the powders [*Barnhoorn et al.*, 2007] results in samples with lengths of 30 mm and diameters of 11.50 mm and porosities <2%. Variation of temperature (between 900 and 1600°C) and duration (24–50 h) of hot isostatic pressing results in samples with different average grain sizes. For all samples the first stage of hot isostatic pressing was performed at 900–1100°C to achieve porosity reduction without excessive grain growth [*Itatani et al.*, 1997]. Samples 1149 (0.9 μm grain size) and 1096 (4.4 μm grain size) have been hot isostatically pressed for 24 h at 900 and 1000°C, respectively. For the two more coarse-grained samples, a 24 h period of hot isostatic pressing at 1100°C was immediately followed by another 24 h at 1300°C during which grain coarsening led to a sample with an average grain size of 8.8 μm (sample 1077). Further heat treatment at 1600°C and 30 MPa confining pressure at hot isostatic pressing facilities at Okayama University of sample 1134 resulted in a sample with an average grain size of 104 μm (Figure 3).

2.2. Mechanical Testing by Forced Torsional Oscillation

Torsional forced-oscillation experiments [*Jackson and Paterson*, 1993] were conducted on each of the four samples at 200 MPa confining pressure over temperature ranges designed to minimize unwanted grain growth as follows: 20–900°C for sample 1149, 20–1100°C for sample 1096, and 20–1300°C for samples 1077 and 1134 (Table 1). Sinusoidally time-varying stresses were applied sequentially at 10 different oscillation periods between 1 and 1000 s at a torque amplitude equivalent to a maximum shear stress of 0.3 MPa, resulting in a maximum shear strain of 3×10^{-5} at the highest temperature. The forced-oscillation data have been corrected for contributions from the mechanical assembly (pistons, metal foils, and steel jacket) to the observed response. Recently improved data reduction procedures [*Jackson et al.*, 2009] for the attenuation apparatus include modeling of the interfacial compliance associated with the $Ni_{70}Fe_{30}$ foils at either end of the specimen, of the mildly viscoelastic behavior of the polycrystalline alumina control specimen, and of any drift in transducer sensitivities,

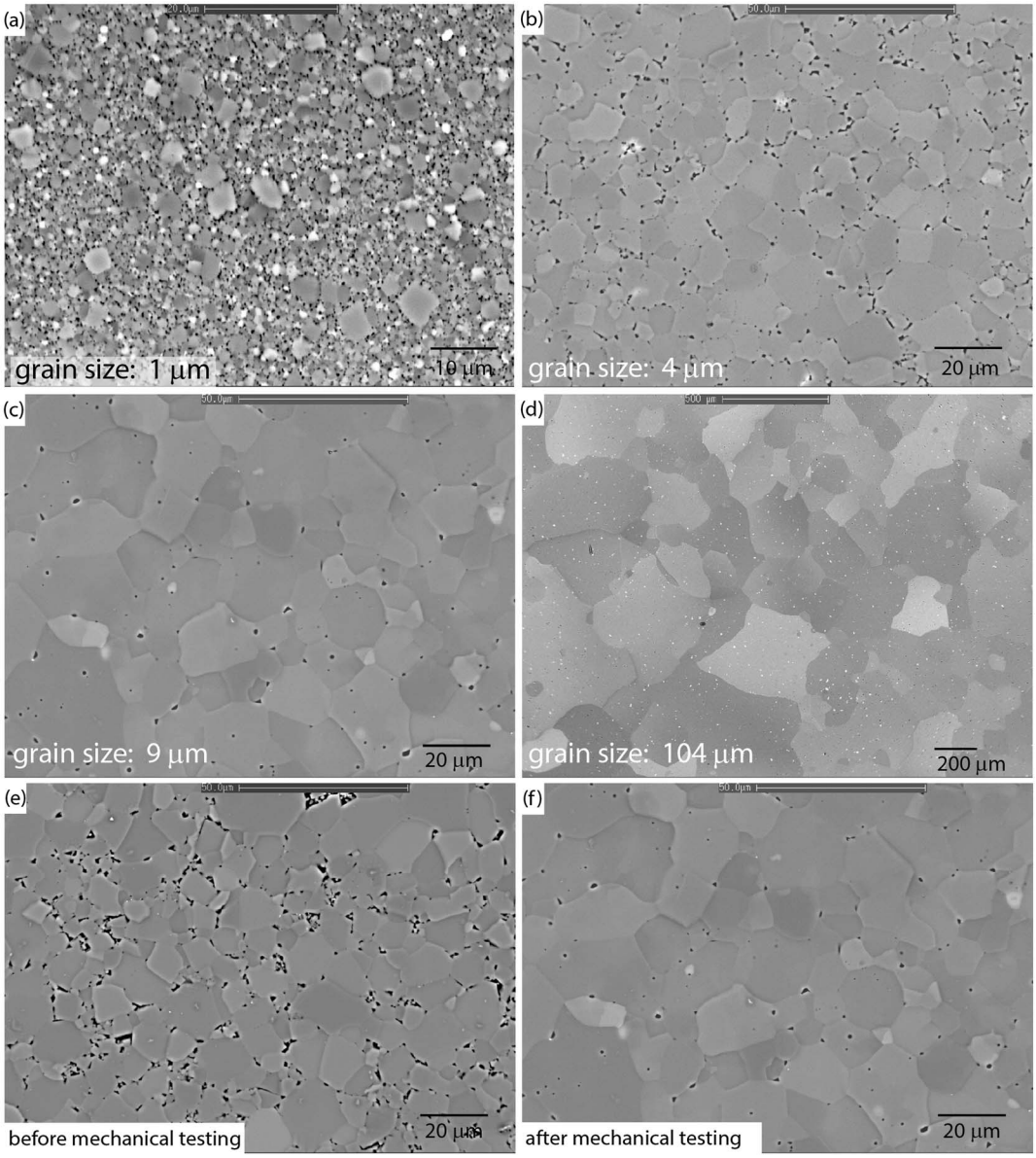

Figure 1. Backscattered electron images of (a) sample 1149 with a mean grain size of 0.9 μm, (b) sample 1096 with a mean grain size of 4.5 μm, (c) sample 1077 with a mean grain size of 8.8 μm, and (d) sample 1134 with a mean grain size of 104 μm. Variations in grey scale levels are due to orientation contrast, not due to compositional variations. Backscattered electron images of sample 1077 (e) before and (f) after mechanical testing indicating minor grain growth and a further minor reduction in porosity during high-temperature mechanical testing.

along with suppression of background creep and the minimization of any aliasing of high-frequency noise. These improved procedures using the double-foil reference assembly have been consistently applied to all four specimens; those data published by *Barnhoorn et al.* [2007] for sample 1077 have been reprocessed for this study. Comparison of the old and new data reduction procedures shows almost indistinguishable results of G and Q^{-1} for two most fine-grained MgO specimens. For the more coarse-grained specimens, the new procedure yields generally higher shear moduli and lower dissipation including some unphysical outcomes at long periods and temperatures $>$ 1100°C, as explained in the notes associated with Figure 4.

Before performing routine torsional forced-oscillation measurements, the samples were annealed in situ at 200 MPa confining pressure at the highest temperature for tens of hours. The mechanical behavior was monitored during annealing. Small changes in shear modulus G and strain energy dissipation Q^{-1} with annealing

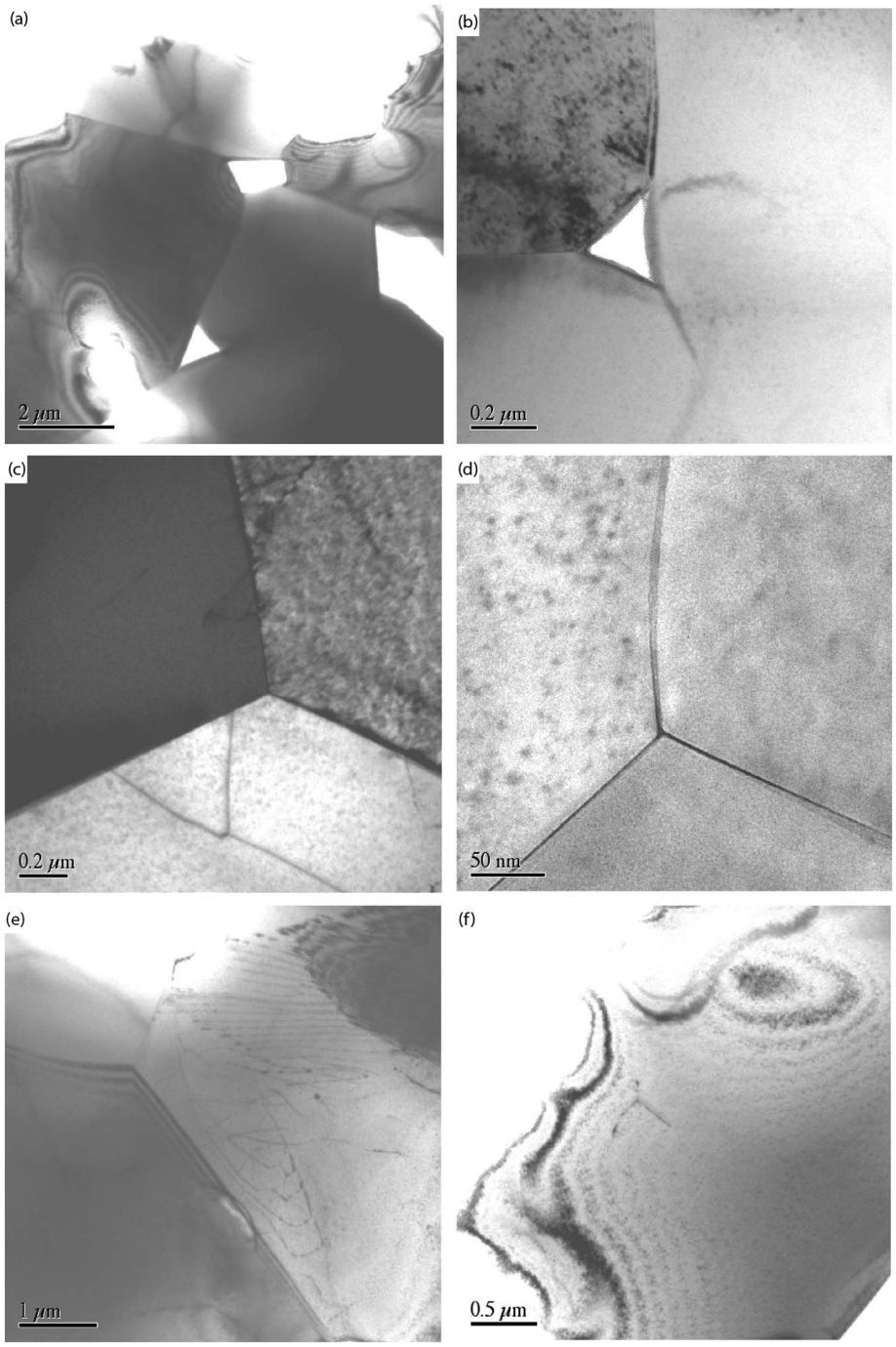

Figure 2. Transmission electron microscopy images of the MgO samples showing presence of (a and b) open pores with sizes between ~50 nm and 1–2 mm suggesting the presence of pressurized fluid, (c) and (d) tight triple junctions in which no pores are present and (e and f) the presence of dislocation walls and isolated dislocations in the interior of some MgO crystals.

time reflect minor microstructural changes, such as an increase in grain size and a further reduction in porosity. This microstructural evolution is primarily confined to the highest temperature, so that mechanical data subsequently acquired during staged cooling reflect the same microstructure. Only for sample 1096 (grain size 4 μm), did revisiting the highest temperature of 1100°C after acquisition of mechanical data during cooling from 1100 to 20°C, reveal changes of mechanical behavior equivalent to a decrease in temperature from 1100°C to 1075°C–presumably reflecting a small amount of microstructural evolution. The other samples can be regarded as measurably constant in microstructure.

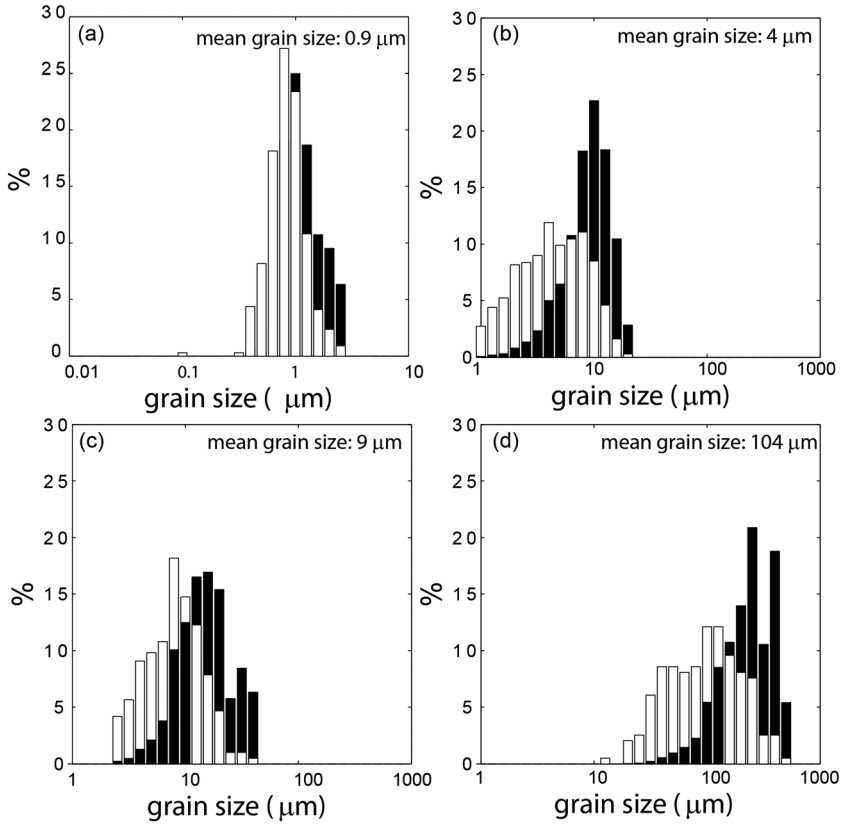

Figure 3. Grain size histograms for (a) sample 1149, (b) sample 1096, (c) sample 1077, and (d) sample 1134. The grain size in microns is calculated from the diameter of the circle equivalent in area to the sectioned grain, with a sectioning correction of $4/\pi$. White bars represent the number frequency distribution of the grain sizes, and the black bars represent the area frequency distribution of the grain sizes. The grain size for each sample used in this manuscript is the mean of the number frequency distribution.

2.3. Burgers Model for the Viscoelastic Relaxation Revealed by Forced Oscillation

The raw forced-oscillation data were converted into shear modulus G, strain energy dissipation Q^{-1}, and shear strain for each period at all temperatures. The shear modulus G and dissipation Q^{-1} data measured on each of the four polycrystals of this study have been fitted to a model for linear viscoelasticity based on a Burgers-type creep function [*Jackson and Faul*, 2010]. In order to ensure a smooth transition between the anelastic and viscous parts of the mechanical relaxation spectrum, the upper end of the range of anelastic relaxation times was here identified with the Maxwell viscous relaxation time $\tau_M = \eta J_U$, where η and J_U are, respectively, the steady state viscosity and unrelaxed compliance. The distribution $D_B(\tau)$ of anelastic relaxation times, used for modeling the monotonic high-temperature background dissipation, thus becomes

$$D_B(\tau) = \alpha\tau^{\alpha-1}/(\tau_M{}^{\alpha} - \tau_L{}^{\alpha}) \tag{3}$$

Table 1. Experiment Details of the Four MgO Samples Indicating Temperature Range of the Forced-Oscillation Experiment and Mean Grain Sizes and Porosity Present in the Mechanically Tested Samples

			Grain Size		
Experiment	Pressure(MPa)	Temperature range(°C)	Number Fraction(μm)	Area Fraction(μm)	Porosity(%)
1149	200	20–900	0.9	1.3	2.28 ± 0.02
1096	200	20–1100	4.5	9.7	1.14 ± 0.02
1077	200	20–1300	8.8	16.5	0.55 ± 0.04
1134	200	20–1300	104	249	0.59 ± 0.04

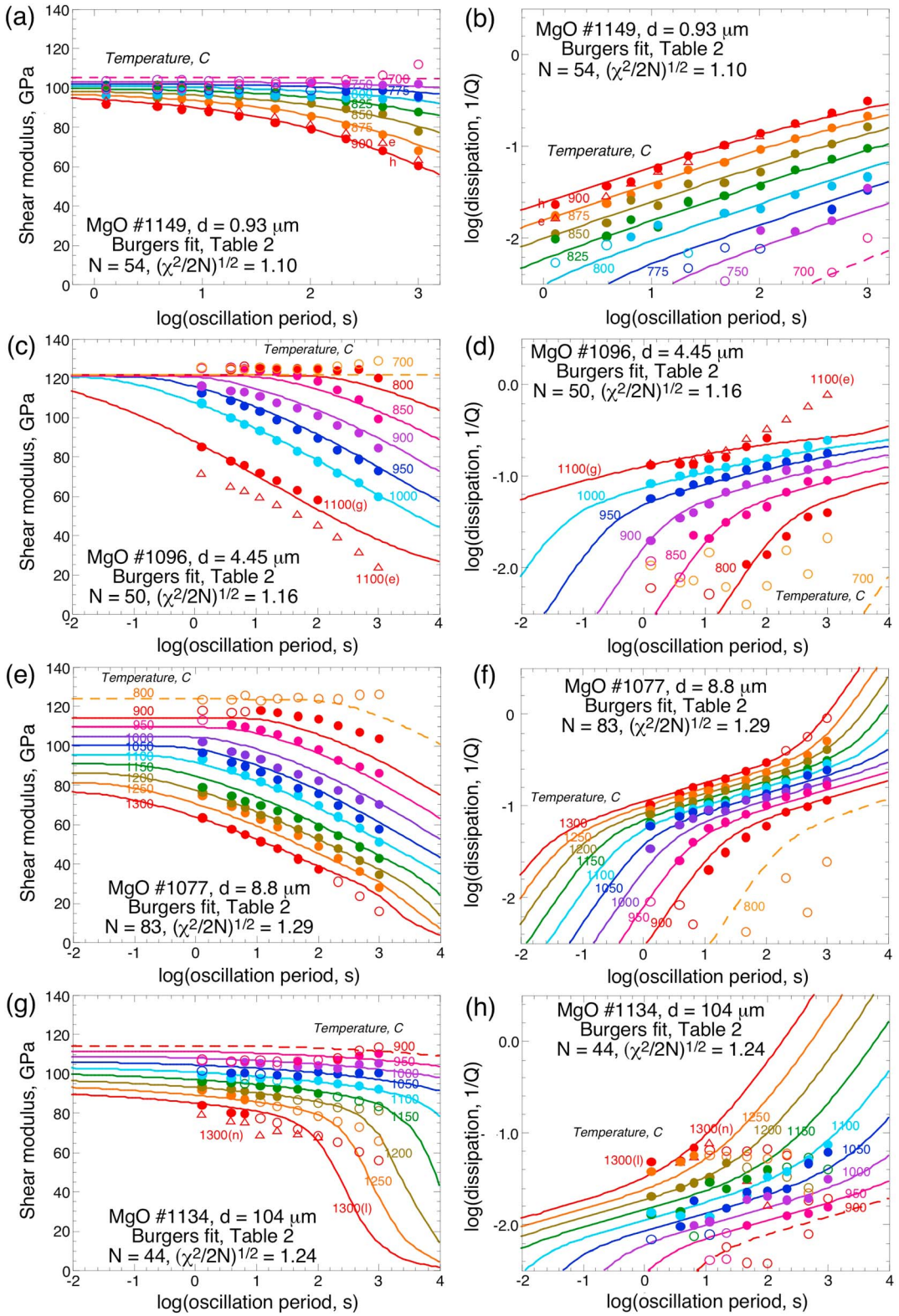

Figure 4. Comparison of the forced-oscillation data for MgO polycrystals 1149, 1096, 1077, and 1134 with the Burgers models of Table 2 (curves) fitted to selected data (denoted by the filled symbols) for each individual specimen—as explained in the notes associated with Table 2. Open symbols indicate data that were excluded from the fits.

with $0 < \alpha < 1$ for $\tau_L < \tau < \tau_M$ and zero elsewhere. Should it be desirable to include in the model a dissipation peak superimposed upon the monotonic background, along with the associated dispersion, the distribution of anelastic relaxation times specified by equation (3) may be augmented by the separately normalized distribution [*Kampfmann and Berckhemer*, 1985; *Jackson*, 2005]

$$D_P(\ln\tau) = \sigma^{-1}(2\pi)^{-1/2}\exp\left\{-[\ln(\tau/\tau_P)/\sigma]^2/2\right\} \tag{4}$$

with relaxation strength Δ_P.

The lower limit τ_L for the distribution of anelastic relaxation times and the Maxwell time τ_M are each referred to the respective value τ_{iR} (with $i = L$ and M) for standard conditions of grain size d_R, temperature T_R, and pressure P_R:

$$\tau_i(T,P,d) = \tau_{iR}(d/d_R)^m\exp[(E_B/R)(1/T - 1/T_R)]\exp[(V^*/R)(P/T - P_R/T_R)]. \tag{5}$$

E_B and V^* are the activation energy and activation volume, respectively. Different values, respectively, m_a and m_v, are allowed for the power law grain size exponents for τ_L and τ_M. The temperature dependence of τ_P for individual specimens is similarly specified with allowance for a distinct value of activation energy E_P. The temperature and pressure dependence of the unrelaxed compliance are specified by

$$J_U(T,P) = [G_U(T_R,P_R) + (T - T_R)\ \partial G_U/\partial T + (P - P_R)\ \partial G_U/\partial P]^{-1}. \tag{6}$$

In using this strategy to fit experimental forced-oscillation data, we have set the reference pressure $P_R = 0.2$ GPa to be that of the forced-oscillation experiments and the reference temperature T_R to 900°C to correspond approximately with the onset of well-resolved anelastic relaxation in medium-grained polycrystalline MgO. In the fits to data for individual specimens, $G_{UR} = G_U(T_R,P_R)$ and $\partial G_U/\partial T$ are treated as adjustable parameters, whereas $\partial G_U/\partial P$ is fixed at the established anharmonic value (2.5). In fitting data for multiple specimens, a seamless transition between elastic and anelastic behavior is imposed by constraining G_{UR} and $\partial G_U/\partial T$ to their unrelaxed values (110.3 GPa and -0.0252 GPa K^{-1}, respectively) inferred from single-crystal measurements at MHz–GHz frequencies [*Anderson and Isaak*, 1995].

2.4. Torsional Microcreep Tests

Torsional microcreep tests complement the forced-oscillation measurements by documenting the extent to which the viscoelastic strain is recoverable upon removal of the applied torque. Each such test, conducted on the same assembly as for the forced-oscillation measurements, involves the application of a torque of amplitude 0, +L, 0, −L, and 0, for successive time intervals typically each of 2000 s duration [*Jackson*, 1993]. The first segment is used to estimate and correct for any linear drift, leaving a four-segment record within which the torque is switched at times t_1, t_2, t_3, and t_4. The switching of the torque can be modeled as the superposition of Heaviside step functions of appropriate sign s_i (+1 at t_1 and t_4, −1 at t_2, and t_3).

The raw microcreep data are first processed to obtain a quantity termed the instantaneous torsional compliance $S_{spc}(t)$, being the time-dependent twist (radian) per unit torque (Nm) for the specimen assembly containing the polycrystalline specimen sandwiched between torsion rods within the enclosing steel jacket. Subtraction of the corresponding twist per unit torque for the reference assembly, $S_{ref}(t)$, in which a control specimen of known properties is substituted for the specimen, eliminates the unwanted contribution from the steel and alumina torsion rods. The difference $S_{rel}(t)$ is the twist of the jacketed specimen relative to the jacketted (Lucalox^{TM} alumina) control specimen, yet to be corrected for any differences in geometry. This difference signal $S_{rel}(t)$ is fitted to a function $S_{fit}(t)$ that is the superposition of the responses to each of the torque switching episodes, prescribed by the appropriate creep function $J(t')$:

$$S_{fit}(t) = \Sigma_{(i=1,k)}s_iJ(t_i') \tag{7}$$

where t_i' is the time elapsed since the ith switching of the torque.

The fit is weighted by specifying an uncertainty in $S_{rel}(t)$ proportional to $\log(t - t_i)$ to weight the data early in each segment relatively more heavily—in order to strengthen the connection with the forced-oscillation data. For reasons of parametric economy, the Andrade creep function is preferred over the Burgers alternative for this purpose

$$J(t') = J_U + \beta t'^n + t'/\eta. \tag{8}$$

The Andrade creep function $J(t)$ associated with this time-domain fit is then Laplace transformed to obtain the corresponding complex dynamic compliance at selected periods (those of the forced-oscillation experiments within the range 1–1000 s). A normally very small correction is then made for any differences in geometry between the two assemblies, to obtain the relative dynamic torsional compliance $S_{rl}(T_o)$. $S_{rl}(T_o)$ is added to the dynamic torsional compliance $S_{jc}(T_o)$ calculated a priori for the jacketted control specimen from unpublished forced-oscillation data for steel and an Andrade pseudoperiod model for the *Lakki et al.* [1998] data for polycrystalline alumina. The result is an estimate of the dynamic torsional compliance $S_{js}(T_o)$ of the jacketted specimen. The reciprocal of S_{js}, the torsional stiffness, is then corrected for the stiffness of the jacket (inclusive of foil wrapper) and inverted to obtain the dynamic torsional compliance $S_s(T_o)$.

At each stage of this process, conducted within the period or frequency domain, the respective dynamic torsional compliance is fitted to an Andrade creep function allowing simulation of the associated microcreep record by superposition of the responses to the successive episodes of torque switching. The results for $S_{rl}(t)$, $S_{jc}(t)$, $S_{js}(t)$, and $S_s(t)$ provide a clear indication of the magnitude of the contributions of the control specimen and jacket to the observed behavior.

The recoverable strain is identified with the βt^n term in the Andrade model, and this fraction f_R of the total inelastic strain $\beta t^n + t/\eta$ can be calculated as function of time t:

$$f_R = \beta t^n/(\beta t^n + t/\eta) = 1/\left(1 + t^{1-n}/\beta\eta\right). \quad (9)$$

Such an estimate can be made for the Andrade model ("fit") fitted to the difference ("rel") between the raw microcreep records right through to the Andrade model fitted to the final $S_s(T_o)$ data—with closely consistent results concerning the fraction of recoverable strain.

3. Results

3.1. Microstructures

Hot isostatic pressing experiments at different maximum temperatures for different durations have produced four high-purity polycrystalline MgO specimens with average grain sizes ranging over 2 orders of magnitude (0.93, 4.45, 8.8, and 104 μm, Figures 1 and 2). All four samples have unimodal grain size distributions. The grain size distribution in the finest grained sample is narrow, progressively widening with an increase in grain size (Figure 3). The average grain sizes reported and used in the fitting of the rheological data refer to mean of the lognormal number distributions of equivalent diameters.

Microstructures of the four specimens (Figure 1) are characterized by equant MgO grains with straight to slightly curved grain boundaries. The grain boundaries have maximum thicknesses of 3–4 nm, and secondary phases in the form of small nanoparticles or thin films are absent. Intergranular pores occurring in the larger MgO grains were presumably incorporated in the grain crystal structure during grain growth. Residual porosity is largest in the most fine-grained specimen: specimen 1149 has a porosity of 2.28% (Figure 1). Pore size varies from ~20 nm to ~20 μm. Detailed transmission electron microscopy (TEM) investigation reveals that around 70% of the triple junctions contain pores (Figure 2). The survival of such pores is indicative of sluggish grain growth, especially in the low-temperature experiments (specimens 1149 and 1096), possibly compounded by the pore pressure of trapped air. TEM investigation on closed pore triple junctions and grain boundaries confirms the absence of any thin amorphous fluid phase along the MgO grain boundaries.

Very few dislocations are present in the MgO grains (Figure 2). Occasionally, however, isolated dislocations occur in large grains with an estimated dislocation density of $\rho \sim 10^{-12}\,m^{-2}$. In the coarse-grained samples, patches of submicron grains are locally situated between larger grains. Those submicron grains have larger dislocation densities with the occurrence of tangled dislocations and dislocation walls. Since the higher dislocation density only occurs in the submicron grains, those dislocations are probably introduced during the early cold isostatic pressing stage of the preparation procedure and have survived the subsequent prolonged high-temperature treatment of the material.

3.2. Forced-Oscillation Data for Individual Specimens

The optimal Burgers model for each of the individual specimens is compared with the corresponding forced-oscillation data in Figure 4. Both the dissipation and the dispersion of the shear modulus are generally well

described by the optimal model for each specimen—consistent with the Kramers-Kronig relationship of linear viscoelastic theory. Broadly subparallel and nearly linear trends on the log-log plots of dissipation against oscillation period, with slopes α of 0.2–0.4, define the anelastic absorption band. Significantly, both ends of the absorption band are evident in the data for specimen 1077 of 8.8 μm grain size. The systematically steeper $\log(Q^{-1}) - \log(T_o)$ trends at short periods for temperatures below 1100°C define the lower end of the anelastic absorption band, associated with the transition from essentially elastic behavior at lower temperatures. At 1300°C, the increasing slope of the $\log(Q^{-1}) - \log(T_o)$ trend at the longest periods heralds the onset of the transition toward viscous behavior. The lower end of the absorption band is also evident in the data for specimen 1096 of 4.4 μm grain size.

The possibility that incorporation of a dissipation peak and associated dispersion might result in an improved fit of the Burgers model to the experimental data has been tested on each of the more extensive data sets (for specimens 1077 and 1096). Use of an additional distribution of anelastic relaxation times specified through equation (4) with the parameters of Table 2 results in a reduction of the average misfit $(\chi^2/2N)^{1/2}$ for each of these specimens but at the cost of four additional, and not consistently well constrained, model parameters Δ_P, $\log\tau_P$, σ, and E_P. Accordingly, the background-only models of Table 2 are preferred, but this exercise demonstrates the inherent difficulty of resolving dissipation peaks of low amplitude superimposed upon a monotonic background.

3.3. A Global Model for Grain Size-Sensitive Viscoelastic Relaxation in MgO

The tendency for the dissipation and associated modulus dispersion to increase with decreasing grain size, for the same temperature and range of oscillation periods, provides the motivation to seek a global model that captures the essential features of the measured variation of G and Q^{-1} with period, temperature, and grain size. The approach was to employ the background-only Burgers model in fitting the composite $N = 131$ data set for specimens 1096 and 1077 of 4.45 and 8.8 μm grain size, respectively (Table 2), and then to compare the predictions of the resulting optimal model with the data for the more fine- and coarse-grained specimens 1149 ($d = 0.93$ μm) and 1134 ($d = 104$ μm). As explained previously, we chose for this purpose to constrain the values of the unrelaxed shear modulus G_U and its temperature derivative $(\partial G_U/\partial T)_P$ at the reference temperature T_R (1173 K) to the well-established high-frequency values. Imposition of these constraints, along with the previously mentioned requirement that $\tau_H = \tau_M$, results in a marginal increase of the misfit but provides a seamless transition between the elastic, anelastic, and viscous regimes, which is preferred especially for later extrapolation to larger mantle grain sizes.

3.4. Comparison of the Global Model With Data for the Medium-Grained Specimens

The resulting model provides a generally satisfactory fit to the (G,Q^{-1}) data for specimens 1077 and 1096 as can be seen in Figures 5 and 6. The model is most tightly constrained by the data for specimen 1077, which are more numerous than for 1096 and also span a wider range of temperature. Both the dissipation and the associated shear modulus dispersion for specimen 1077 are well represented by the model—but less so the absolute values of the shear modulus that are somewhat more variable between adjacent temperatures—on account of uncertainties in the calibration factors for the displacement transducers (Figure 6). The model similarly provides a generally adequate representation of the data for specimen 1096, which are both fewer and confined to a narrower temperature range (800–1100°C). However, at temperatures of 850–950°C and short periods, both the dissipation and associated dispersion are somewhat underestimated.

3.5. Implications for the More Fine- and Coarse-Grained Specimens

Also shown in Figure 6 are the results of evaluating the global model at the grain sizes appropriate for the more fine- and coarse-grained specimens: 1149 (0.93 μm) and 1134 (104 μm). The fact that the grain size increases only twofold between 1096 and 1077 means that grain size sensitivity m_a of the anelastic relaxation times in this model may not be particularly well constrained.

3.5.1. Specimen 1134 ($d = 104$ μm)

For the most coarse-grained specimen 1134, the inferred period dependence of the dissipation becomes negative at sufficiently long periods and high temperatures—an effect that is less than physically plausible, and is attributed to underestimation of the strength of the viscoelastic relaxation in the polycrystalline alumina control specimen, as noted previously. However, for the shorter-period high-temperature data and those for lower temperatures, any reduction in apparent dissipation (and associated dispersion) is evidently

Table 2. Burgers Creep Function Models Fitted to N (G,Q^{-1}) Pairs of Data for Each of the Individual MgO Polycrystals, Including That of *Webb and Jackson* [2003], Along With a Global Model Fitted to Data for Specimens 1096 and 1077[a]

Fit	1149	1096	1096	1077	1077	1134	**1096** and **1077**	W&J 2003
N	54[b]	50[c]	50	83[d]	83	44[e]	**131**[f]	91[g]
d_R (μm)	0.93	4.45	4.45	8.8	8.8	104.0	**6.26**	55
T_R (K)	1173	1173	1173	1173	1173	1173	**1173**	1173
P_R (GPa)	0.2	0.2	0.2	0.2	0.2	0.2	**0.2**	0.2
V^* (cm^3 mol^{-1})	10	10	10	10	10	10	**3**	3
$G_U(T_R,P_R)$ (GPa)	96.7(7)	121.0(5)	122.0(7)	114.1(8)	117.1(9)	114.0(11)	[**110.3**]	86.7(7)
$\partial G_U/\partial T$ (GPa K^{-1})	−0.041(10)	−0.003(2)	[−0.0252]	−0.094(4)	−0.071(5)	−0.056(5)	[−**0.0252**]	−0.015(5)
Δ_B	[2]	3.55(1)	[3]	1.37(5)	1.58(8)	0.22(2)	**1.76**(**4**)	[1.3]
α	0.409(9)	0.224(3)	0.48(4)	0.266(9)	0.335(12)	0.192(16)	**0.206**(**5**)	0.323(13)
$\log_{10}\tau_{LR}$(s)	[−3]	−0.56(3)	[−1.5]	0.33(6)	0.48(12)	[0]	**0.29**(**4**)	[−3]
$\log_{10}\tau_{MR}$(s)	3.64(4)	6.31(1)	5.22(11)	4.71(8)	4.87(9)	[6.3]	**5.55**(**5**)	3.65(6)
Δ_P			0.47(4)		0.18(2)			0.87(5)
$\log_{10}\tau_{PR}$(s)			2.02(7)		3.25(15)			2.23(13)
σ			[3]		[2.9]			3.21(24)
m_a							**1.1**(**2**)	
m_v							[**3**]	
E_B (kJ mol^{-1})	488(11)	473(1)	379(13)	248(8)	264(8)	432(7)	**391**(**4**)	185(8)
E_P (kJ mol^{-1})			[520]		[750]			599(28)
χ^2_G	15.8	55.5	29.8	176.5	125.3	14.6	**378.9**	172.2
$\chi^2_{1/Q}$	115.1	80.1	38.2	101.3	29.3	121.6	**404.0**	79.2
χ^2_{tot}	130.9	135.6	68.0	277.8	154.6	136.3	**782.8**	251.4
$(\chi^2_{tot}/2N)^{1/2}$	1.10	1.16	0.82	1.29	0.97	1.24	**1.73**	1.17

[a]For each specimen, all (G,Q^{-1}) data pairs with $\log(Q^{-1}) > \approx -2.0$, indicated by filled plotting symbols in Figure 4 (rev), were fitted to an optimal Burgers creep function model. Data excluded from the fit are indicated by open symbols in Figure 4. A priori errors were set to $\sigma(G)/G = 0.03$, $\sigma[\log(Q^{-1})] = 0.05$.

[b]Temperature interval: 900–750°C inclusive. The close consistency between the "e" data obtained at 900°C after a prolonged period of annealing prior to staged cooling, and the "h" data obtained on return to 900°C following staged cooling to room temperature, suggests that there was no significant microstructural evolution following the initial period of annealing at 900°C (Figures 4a and 4b).

[c]Revisiting of the highest temperature (1100°C) for this specimen following staged cooling to room temperature revealed significantly higher moduli and somewhat lower dissipation (data labeled "g" in Figures 4c and 4d) than those (e) measured following annealing at 1100°C prior to staged cooling. The later 1100°C data were combined with the staged-cooling data for the temperature range 1000–800°C, exclusive of short-period data at 850 and 800°C.

[d]Annealing for 49 h at 1300°C was followed by staged cooling to room temperature but without subsequent return to the maximum temperature; data obtained across the temperature range 1300–900°C were fitted (Figures 4e and 4f).

[e]Data at the highest temperatures and longest periods are affected by uncertainties in the viscoelastic behavior of the Lucalox alumina control specimen; accordingly such data are excluded from the fit (Figures 4g and 4h). The values of G and Q^{-1} observed on revisiting 1300°C following the staged cooling to room temperature (denoted "n") are closely comparable with those obtained following prolonged annealing (114 h) at 1300°C prior to the onset of staged cooling ("l"), suggesting very little microstructural evolution in this specimen during the main phase of mechanical testing. Anomalously high shear moduli for $T \leq 1000$°C are reflected in a value of G_{UR} significantly greater than the anharmonic value.

[f]Data for specimens 1096 and 1077 as described in footnotes b and c, except for exclusion of two additional data pairs for specimen 1096, involving low levels of dissipation at short periods and low temperatures of 850 and 800°C (retaining data for $T_o \geq 11.5$ s and ≥ 101 s, respectively).

[g]Data reported by *Webb and Jackson* [2003] for all periods between 1.02 and 100.4 s at temperatures equally spaced at 50°C intervals between 1300 and 700°C, reprocessed as described in the text.

less severe. These latter data are quite well approximated by the global Burgers model fitted to the data for specimens 1096 and 1077—notwithstanding the long extrapolation of the model to 104 μm grain size. Unsurprisingly then, expansion of the data set to $N = 175$ by including the 44 "robust" (G,Q^{-1}) pairs for specimen 1134 resulted in a global model not very different from that of Table 2, with $(\chi^2/2N)^{1/2} = 1.80$, but with a substantially inferior fit to the lower end of the anelastic absorption band, which is apparently well resolved by the data for specimens 1096 and 1077.

3.5.2. Specimen 1149 ($d = 0.93$ μm)

The testing of the most fine-grained specimen 1149 was restricted to temperatures ≤900°C in order to minimize grain growth. As a result, there is minimal overlap with the temperature range for appreciable viscoelastic relaxation in the more coarse-grained materials—somewhat complicating a meaningful comparison. However, it is clear from Figure 6 that for temperatures of 800–900°C, within which range the two data sets overlap, specimen 1149 of 0.93 μm average grain size is only marginally more lossy than specimen 1096 of significantly greater grain size (4.4 μm). Consequently, the global model fitted to the data for specimens 1096 and 1077 substantially overestimates both the observed dispersion and dissipation for the most fine-grained specimen 1149.

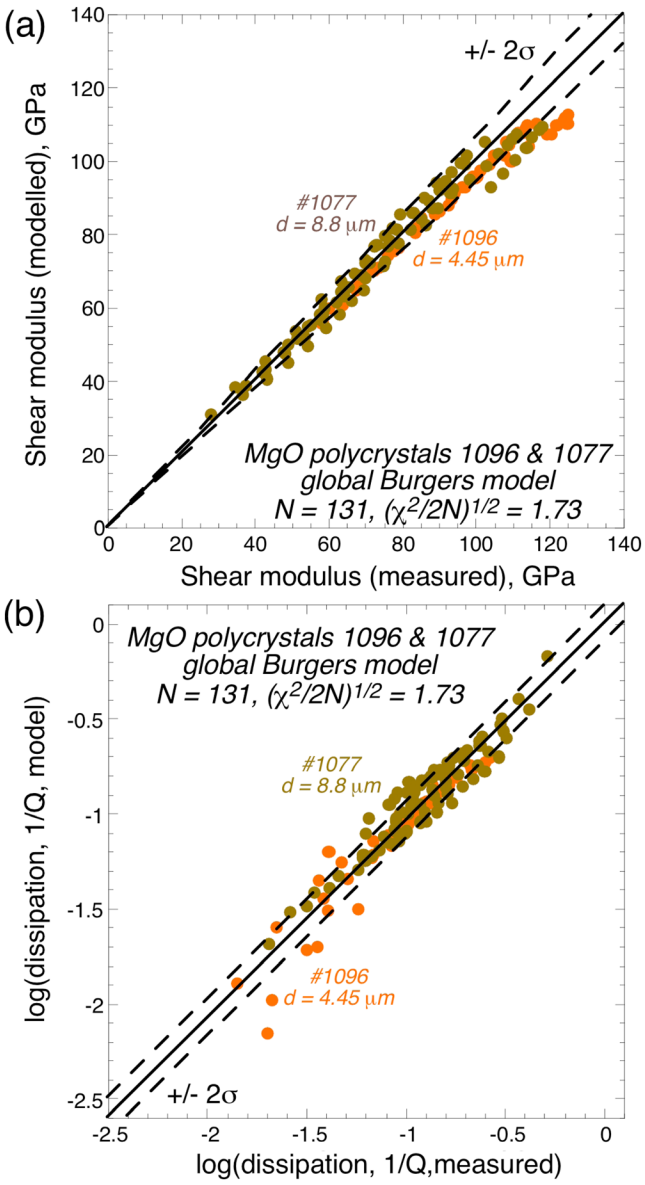

Figure 5. A comparison of the shear modulus and dissipation data for specimens 1096 and 1077 with those of the global model (Table 2, bold column). The data are generally consistent with the model within $\pm 2\sigma$ ($\sigma(G)/G = 0.03$, $\sigma[\log(Q^{-1})] = 0.05$).

3.6. The Preferred Global Model

Accordingly, it is concluded that the global model of Table 2 provides an adequate fit to the most robust data for specimens 1096 and 1077 including the well-resolved lower end of the anelastic absorption band, and also a satisfactory approximation to the dissipation and dispersion measured on the coarse-grained specimen 1134. This model provides a reasonable fit to the period, temperature, and grain size sensitivity of shear modulus and dissipation across a substantial range of each of these variables (Figure 6) but is clearly unreliable at smaller grain sizes. Although follow-up work on coarse-grained materials would be highly desirable, the global model of the present study can be used in the meantime to provide interim estimates of the dispersion and dissipation to be expected at larger grain sizes, such as those of the Earth's mantle.

3.7. Representative Results From Complementary Torsional Microcreep Tests

The results of a representative torsional microcreep test are displayed in Figure 7. The trend labeled "spc" in Figure 7a represents the appreciably viscoelastic response of the specimen assembly to the series of torque switchings. In addition to the instantaneous elastic distortion associated with each such change of the torque, there is clearly a delayed recoverable (i.e., anelastic) component of the distortion, along with some permanent deformation. The response S_{ref} of the reference assembly is more mildly viscoelastic, and its subtraction from S_{spc} yields S_{rel}, the torsional compliance of the jacketed specimen relative to the jacketed (alumina) control specimen. Following the previously described fitting of this difference signal to the Andrade model, labeled fit in Figure 7a, the data processing continues in the period domain. S_{fit} is first corrected for minor differences in geometry between the specimen and control specimen to obtain S_{rl} (Figure 7b). Then S_{rl} is added to the calculated compliance S_{jc} of the jacketed control specimen to obtain the compliance of the jacketed specimen S_{js}, and its inverse the torsional stiffness, from which the effect of the jacket can be removed leaving finally the response labeled "s" of the specimen itself.

The microcreep record thus obtained for the specimen retains the essential character of the raw data labeled spc in Figure 7a. Moreover, the fraction of recoverable strain can now be quantified, as explained previously, from the coefficients of the corresponding Andrade model (equation (9)). The results are shown

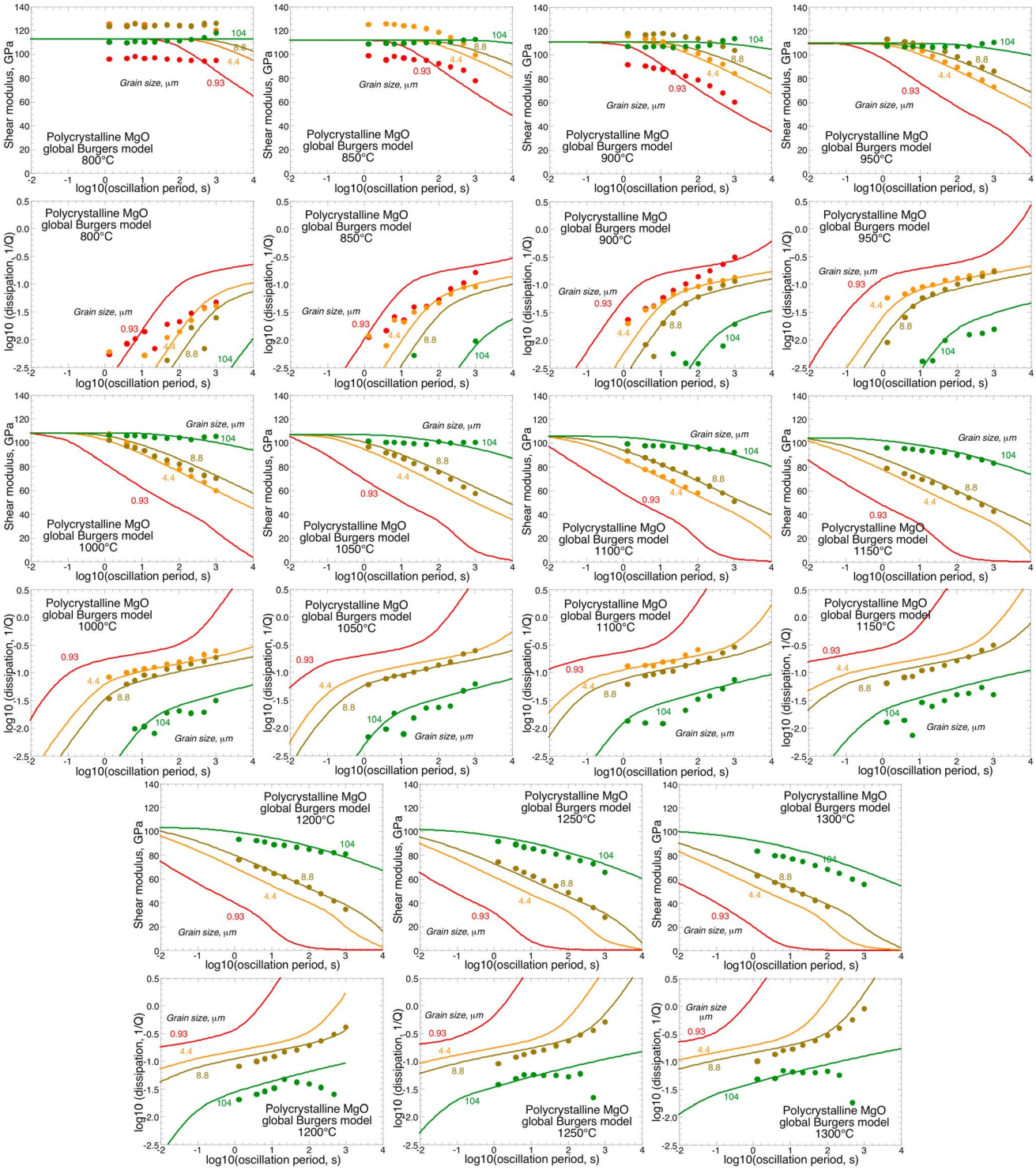

Figure 6. The grain size sensitivity of viscoelastic relaxation in polycrystalline MgO, as specified by the global Burgers model (Table 2, bold column). The values of shear modulus and shear-mode dissipation measured in forced torsional oscillation at the indicated temperatures on specimens 1149 (0.93 μm), 1096 (4.4 μm), 1077 (8.8 μm), and 1134 (104 μm) are indicated by the red, orange, khaki, and green plotting symbols, respectively. The curves representing the Burgers model are similarly color coded.

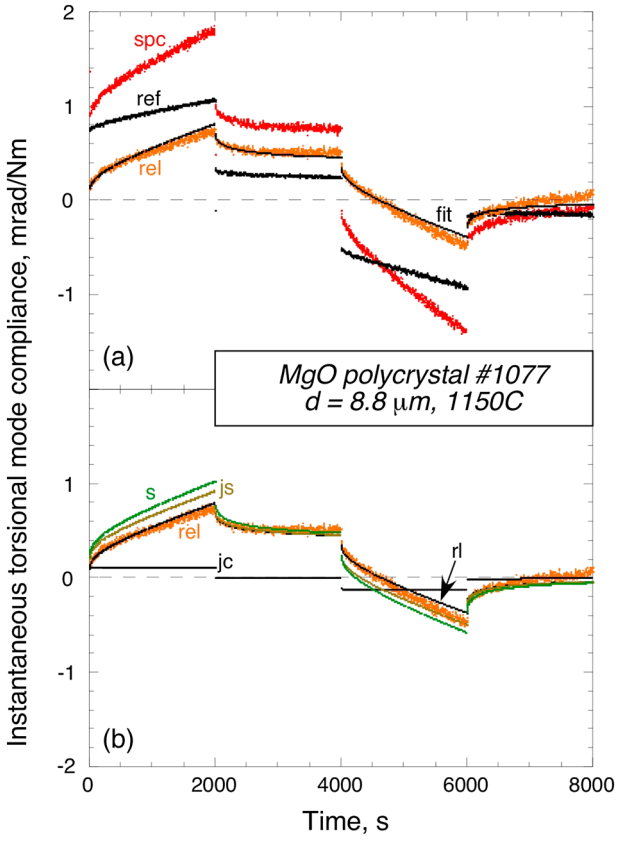

Figure 7. The results of a representative torsional microcreep test conducted on specimen #1077 at 1150°C. (a) The instantaneous torsional compliance S_{spc} and S_{ref} for the specimen and reference assemblies are labeled "spc" and "ref," respectively, while their difference S_{rel} and its optimal Andrade fit are labeled rel and fit, respectively. (b) The difference between the compliances of the specimen and reference assemblies is reproduced from Figure 7a, whereas the trends labeled "rl," "jc," "js," and "s" represent the time-domain implications of the period domain calculations described in the text.

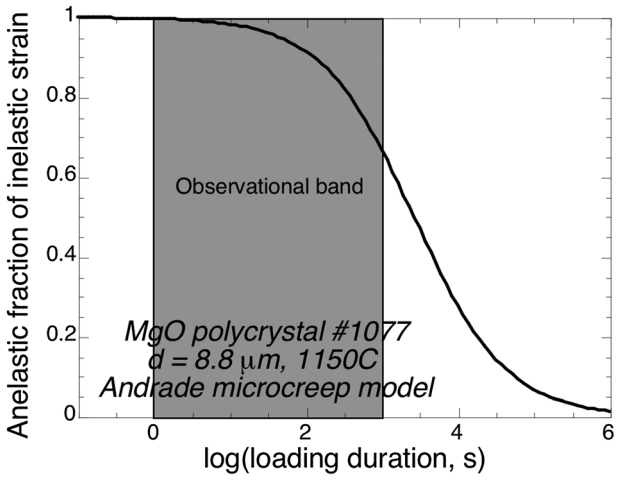

Figure 8. The recoverable (anelastic) fraction of the inelastic deformation of the specimen calculated from equation (9) for the Andrade model for S_s.

in Figure 8, where it is evident that the response at short times is largely anelastic with a progressive decrease in the anelastic fraction of the nonelastic deformation with increasing time/period to approximately two thirds at the long-period end of the observational/seismic band. In principle, the shear modulus and dissipation for the specimen can be inferred from the Laplace-transformed microcreep records. However, a close comparison of this kind between the forced-oscillation and microcreep data will require consistent analysis of both data sets with the same, preferably Burgers, creep function model—a target for future work.

4. Discussion

4.1. Influence of Porosity on Viscoelastic Relaxation

Imaging of the MgO samples by transmission electron microscopy reveals that the majority of the grain triple junctions contain small pores (pore size 20 nm–20 μm). Existence of pore spaces even after tens of hours at high pressures is due to either the sluggish grain growth of MgO or the presence of a fluid/gas phase exerting a pore pressure acting against the confining pressure. In the finer-grained samples (1149 and 1096), the presence of residual porosity can be explained by sluggish grain growth at low temperatures. In the two more coarse-grained samples, the low porosity is concentrated on the triple junctions of grains. It is expected that grain growth over the long experimental durations at high temperatures, tens of hours, should have removed all residual porosity by grain growth, unless a gas/fluid pressure was present. Although it is thus inferred that a fluid/gas phase may have been present in the pore space, the pores were probably isolated, and any involvement of the pore space in the observed viscoelastic behavior is considered negligible.

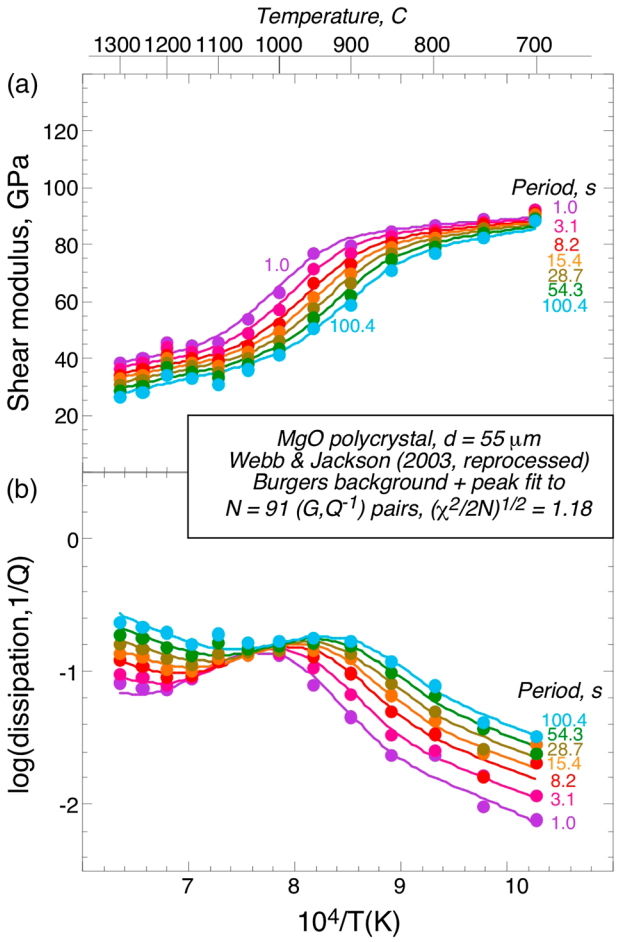

Figure 9. The forced-oscillation data of *Webb and Jackson* [2003] for a mildly impure MgO polycrystal of 55 μm average grain size, newly reprocessed with allowance for the interfacial compliance associated with the foil grips at each end of the specimen [*Jackson et al*., 2009]. (a) Shear modulus and (b) log (dissipation) versus reciprocal temperature. Data are indicated by the plotting symbols, whereas the curves represent the optimal Burgers background-plus-peak model (Table 2) as described in the text. Both plotting symbols and curves are color coded according to oscillation period between 1 and 100 s.

4.2. Comparison With Previous Studies of Polycrystalline MgO

4.2.1. Forced-Oscillation Measurements of *Webb and Jackson* [2003]

Forced-oscillation data for a mildly impure MgO polycrystal of 55 μm grain size, reported by *Webb and Jackson* [2003], were compared with the data for specimen 1077 by *Barnhoorn et al*. [2007]. In order to facilitate closer comparison with the results of the present study, the data of *Webb and Jackson* [2003], newly reprocessed with allowance for the interfacial compliance associated with the foil grips at each end of the specimen [*Jackson et al*., 2009], are presented in Figure 9. As previously suggested by *Barnhoorn et al*. [2007], the *Webb and Jackson* [2003] data reveal a pronounced dissipation peak superimposed upon a dissipation background which varies monotonically with oscillation period and temperature, along with enhanced period dependence (dispersion) of the shear modulus. The full set of dissipation and modulus data is well described by a Burgers model of the type used to fit the data of the present study but with an additional log-normal distribution of anelastic relaxation times (equation (4)) specified by the following parameters: Δ_P, $\log\tau_{PR}$, σ, and E_P (Table 2 and Figure 9). This model clearly captures the key observation, namely that with increasing temperature; the center of the dissipation peak traverses the observational window of oscillation periods from 100 s period at 900°C to 1 s at 1050°C. Superposition of the peak upon the period-dependent background results in a prominent dissipation plateau at $\log Q^{-1} \sim -0.8$ for periods of 1–100 s and temperatures of 1000–1050°C. Such behavior contrasts markedly with the results from the present study on pure MgO polycrystals which exhibit much lower and monotonically period-dependent dissipation under similar conditions (Figure 4). By analogy with similar observations for melt-bearing polycrystalline olivine, the dissipation peak observed in the *Webb and Jackson* [2003] data was attributed by *Barnhoorn et al*. [2007] to the presence of an intergranular fluid phase associated with a substantial concentration of impurities.

4.2.2. Torsional Pendulum Study of *Pezzotti* [1999]

The results of a torsional pendulum study, involving the testing of MgO polycrystals of average grain size 5, 11.2, and 22.5 μm at temperature-insensitive resonance frequencies near 3, 13, and 20 Hz, were reported by *Pezzotti* [1999]. Because such (essentially isochronal) data were acquired over very wide ranges of temperature (~1000–2000°C), it was possible in $\log(Q^{-1}) - 1/T$ space to distinguish a broad dissipation peak from a background dissipation with an Arrhenian temperature dependence (Figure 10a, see, however, the discussion in Appendix A). High-temperature background dissipation is commonly parameterized as $Q_{bg}^{-1} \propto (\omega\tau)^{-\alpha}$, where τ is an appropriate thermally activated relaxation time (e.g., equation (2)) with activation energy E_B, and α is an

exponent typically between 0.2 and 0.5. Under these circumstances, $\partial \log Q_{bg}^{-1}/\partial(1/T) = -\alpha E_B/R \ln 10$, where R is the gas constant. For the only complete set of background plus peak dissipation data published by *Pezzotti* [1999] (Figure 10a), the inferred slope of -8700 K yields an apparent activation energy αE_B of 167 kJ mol^{-1}. Unambiguous determination of E_B would require information concerning the frequency dependence of the background dissipation, unfortunately not reported by *Pezzotti* [1999].

The dissipation peak, isolated by subtracting the fitted Arrhenian background from the measured dissipation (Figure 10a), was found to vary systematically in position (temperature) with changing resonance frequency and grain size [*Pezzotti*, 1999]. If the dissipation peak is crudely approximated by a Gaussian function of the logarithm of pseudoperiod X given by

$$X = (1/f)(d/d_r)^{-m} \exp[-(E_P/R)(1/T - 1/T_r)] \tag{10}$$

with appropriate mean and standard deviation [*Jackson*, 2005], then the sensitivities of peak position δT_P to changing frequency δf and grain size δd are found by requiring $\delta X = 0$. It follows that

$$\delta T_P\big|_d \approx \left(RT_P^2/E_P\right)\delta \ln f \quad \text{and} \quad \delta T_P\big|_f \approx \left(mRT_P^2/E_P\right)\delta \ln d \tag{11}$$

from which expressions, values of $E_P \sim 160$ kJ/mol and $m = 0.7$ can be inferred.

This value for the activation energy for the relaxation time associated with the dissipation peak is strikingly similar to that (167 kJ/mol) of αE for the dissipation background observed by *Pezzotti* [1999], suggesting that the background and peak dissipation may be subject to similar thermal activation. For the global model of the present study, the value of αE is markedly lower at 82 kJ/mol. The value $m = 0.7$ inferred from the grain size sensitivity of the peak position in the *Pezzotti* [1999] study is not markedly different from that (1.1(2)) of the global model of the present study and broadly compatible with the expectation of $m = 1$ for the relaxation time for elastically accommodated grain boundary sliding (section 1).

Pezzotti's [1999] model thus involves the superposition of a (compound) dissipation peak of modest amplitude ~ 0.03 upon an Arrhenian background—resulting in a seamless transition between a broad anelastic dissipation peak and essentially viscous behavior (Figure 10a). In the Burgers model of the present study, the anelastic absorption band is specified instead with a continuous distribution of relaxation times between lower and upper limits with a common temperature and grain size sensitivity, similarly providing a smooth transition between anelastic and viscous behavior (e.g., Figure 6). The fact that the frequency and grain size sensitivities of the Arrhenian background are not specified for *Pezzotti's* [1999] model precludes a broad comparison of the results from *Pezzotti* [1999] and present studies. Under these circumstances, it is most instructive to compare the most complete of the *Pezzotti* [1999] data sets (for $d = 5\ \mu$m and $f = 13$ Hz) with the data from the present study for the specimen of comparable grain size ($d = 4.45\ \mu$m). The raw data from the two studies are compared in Figure 10b, where the fit to the data for specimen 1096 is also extrapolated to 0.0769 s period (13 Hz) for direct comparison with the *Pezzotti* [1999] data.

Although there is a substantial offset between the *Pezzotti* [1999] data and the extrapolation of $Q^{-1}(1/T)$ from the longer periods of this study, the remarkably similar shapes of the $\log Q^{-1}(1/T)$ trends suggest that the edge of the anelastic absorption band, at low temperatures and short periods (Figures 4 and 6), is a well-resolved feature of the viscoelastic behavior. Despite its different (subresonant) methodology and longer oscillation periods, the present study, through its clear observation of a sharp low-temperature short-period edge for the anelastic absorption band, reinforces one of the most robust findings of the previous work by *Pezzotti* [1999]. Such dissipation peaks, plausibly associated with elastically accommodated grain boundary sliding, have generally been conspicuous by their absence in other fine-grained materials of high purity, at least until recently [*Jackson et al.*, 2014]. The findings for MgO, and indeed Al_2O_3 polycrystals [*Pezzotti*, 1999], reinforce the suggestions from micromechanical models [*Lee et al.*, 2011; *Jackson et al.*, 2014] that dissipation localized in frequency/temperature space as a broad peak with amplitude of order 10^{-2} may be characteristic of the transition from elastic to anelastic behavior in fine-grained ceramics. Superposition of such a peak upon the mild power law frequency dependence of the diffusionally assisted high-temperature background will typically result in a shoulder or plateau observable amongst $Q^{-1}(\omega)$ data.

4.2.3. Steady State Diffusional Creep

The surprising scarce literature concerning diffusional creep of polycrystalline MgO has been assessed by *Frost and Ashby* [1982]. Their preferred flow law yields a viscosity markedly higher and more mildly

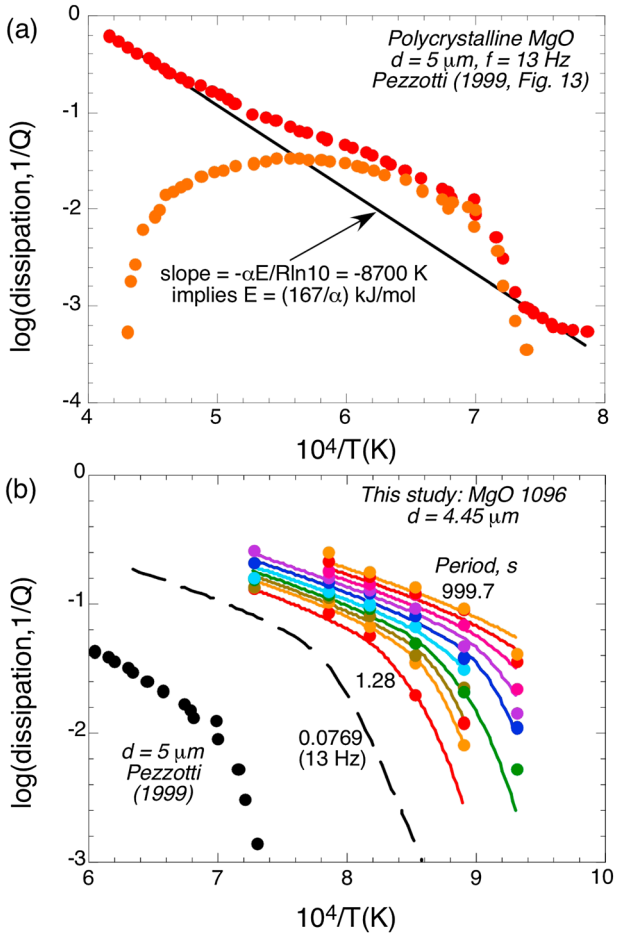

Figure 10. (a) Dissipation (red plotting symbols) measured at 13 Hz for polycrystalline MgO of 5 μm grain size, interpreted by *Pezzotti* [1999] as an Arrhenian background (black line) with a superimposed dissipation peak (orange symbols). (b) Comparison of *Pezzotti's* [1999] torsional pendulum data ($d = 5$ μm, $f = 13$ Hz, black plotting symbols) with those (colored symbols) obtained in the present study at forced-oscillation periods > 1 s on a specimen #1096 of similar grain size. Extrapolation of the Burgers model (curves color coded for period) fitted to the data for specimen 1096 (Table 2) to 13 Hz yields the broken black curve.

temperature dependent than does the Burgers model of the present study (Figure 11). The Maxwell relaxation time $\tau_M = \eta J_U$ of the Burgers model, fitted to the torsional forced-oscillation data, is constrained only by the steepening period dependence of dissipation for periods > 100 s at temperatures ≥ 1200°C for specimen 1077 of 8.8 μm grain size. Such microstrain data have been interpreted as indicative of the beginning of the transition from diffusionally assisted toward diffusionally accommodated grain boundary sliding. However, it is clear from Figure 8 that the behavior remains overwhelmingly anelastic under these conditions. The serious underestimate of the steady state viscosity is accordingly unsurprising.

4.3. Interim Extrapolation of the Preferred Global Model to Mantle Grain Sizes and Pressure-Temperature Conditions

For an indicative extrapolation of the global Burgers model of the present study (Table 2) to a pressure 23 GPa representative of the uppermost lower mantle where ferropericlase (magnesiowüstite) coexists with the silicate perovskites, the value ($3\,cm^3\,mol^{-1}$) of the activation volume V^* reported by *van Orman et al.* [2003] is used, resulting in an increase of ~70 kJ mol^1 in the activation enthalpy $H = E + PV^*$ between 0.2 and 23 GPa. The values of shear modulus and dissipation calculated from the model at 23 GPa pressure, grain sizes of 1, 10, and 100 mm, and representative temperatures are shown in Figure 12.

In assessing the results of these extrapolations, it is necessary to consider the impact of the grain size exponents for the various relaxation times. The fact that the exponent $m_a = 1.1(2)$ for τ_L, the relaxation time defining the lower end of the anelastic absorption band is significantly smaller than that ($m_v = 3$, relevant for Coble creep) associated with the Maxwell relaxation time τ_M, results in a broadening of the anelastic absorption band with increasing grain size, as follows. It follows from equation (4) that the width of the anelastic absorption band, under any prescribed conditions of pressure and temperature, is a function only of grain size, specifically

$$\log[(\tau_M/\tau_L)(d)]|_{T,P} = \log[(\tau_{MR}/\tau_{LR})] + (m_v - m_a)\log[d/d_R]. \quad (12)$$

Extrapolation of the global Burgers model to larger grain sizes, therefore, results in a systematic broadening of the anelastic absorption band (Figure 13). It can be concluded from Figure 12 that seismic and tidal frequencies are likely to probe only the anelastic part of the mechanical response of lower mantle ferropericlase.

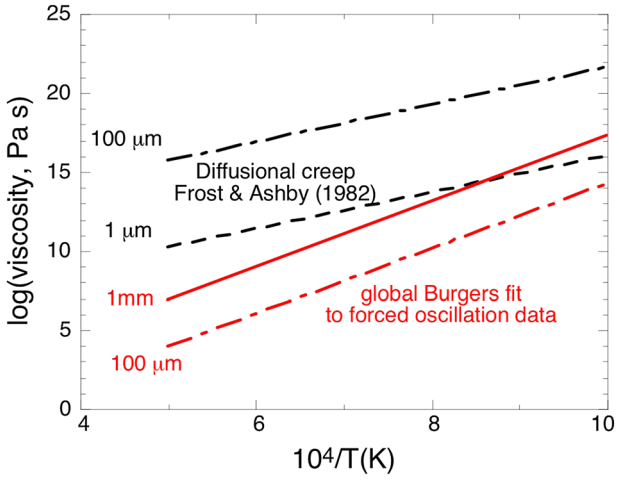

Figure 11. Comparison of the Arrhenian temperature dependencies of viscosity for polycrystalline MgO as prescribed by the diffusional creep flow law of *Frost and Ashby* [1982] and inferred from the Burgers model of Table 2 fitted to the torsional forced-oscillation data of the present study.

Only for the smallest grain size of Figure 12 (1 mm) does the Maxwell relaxation time (2×10^8 s ~ 6 year at 1500°C) approach the upper end of the tidal frequency band. The predicted convergence between τ_M and τ_L for grain sizes significantly less than d_R calls into question the existence of an anelastic absorption band in ultrafine-grained materials.

Concerning the effect of pressure, at fixed grain size and temperature, it follows from equation (4) that

$$\log[\tau_i(P)/\tau_i(P_R)]|_{d,T} = (P-P_R)V^*/RT\ln 10. \quad (13)$$

Accordingly, the effect of the increased pressure from 0.2 GPa in the laboratory tests to 23 GPa in the uppermost lower mantle (Figure 12) is to displace the $\log Q^{-1}$ versus log (period) contours for a given temperature to longer periods. The displacement calculated from equation (13) varies from 2.4 log units at 1200°C to 1.8 log units at 1700°C. The resulting higher-temperature sensitivity of dissipation at the higher pressure is consistent with the increased enthalpy.

Use of the linear pressure dependence of G_{UR} prescribed by equation (5) for the lengthy extrapolation in pressure, rather than a more appropriate finite strain formulation, will consistently overestimate the shear moduli plotted in Figures 12a–12c but not seriously affect the calculated dispersion.

4.4. Implications for the Lower Mantle Perovskite + Ferropericlase Mixture

The mineralogy of the Earth's lower mantle is expected to be dominated by Mg-silicate perovskite (bridgmanite), comprising ~70% of the mineral assemblage, with ferropericlase next most abundant at

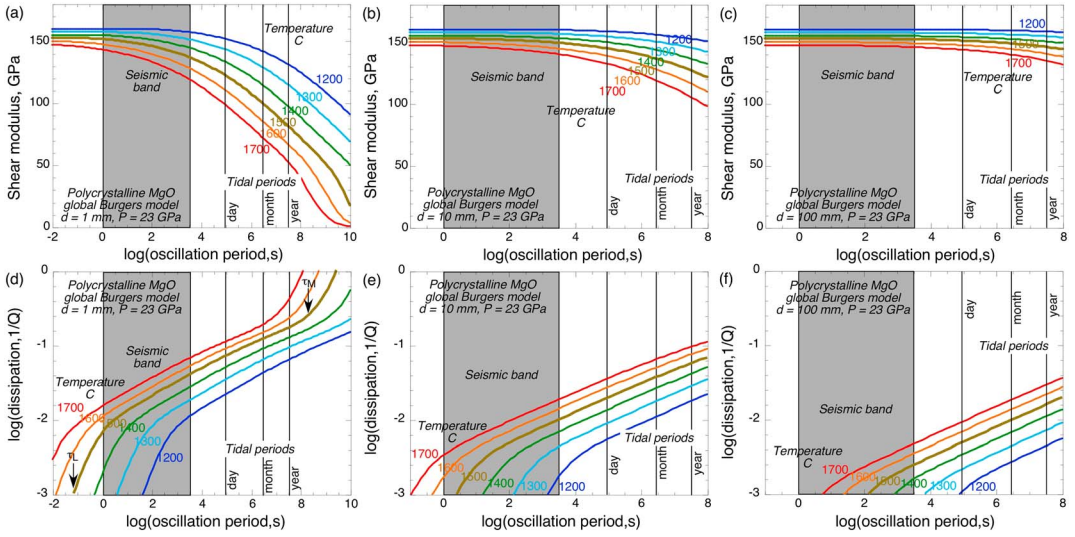

Figure 12. The global model for the viscoelastic behavior of polycrystalline MgO evaluated for a broad range of periods at the larger grain sizes of 1, 10, and 100 μm and the uppermost lower mantle pressure of 23 GPa. The results for 1500°C, represented by the bold ochre curves, are emphasized because this temperature approximates that associated with the mantle adiabat at 23 GPa. The extrapolation of relaxation times in pressure is based on an activation volume V^* of 3 cm^3 mol^{-1} [*van Orman et al.*, 2003]. (a–c) Shear modulus at grain sizes of 1, 10, and 100 mm, respectively. (d–f) Dissipation at grain sizes of 1, 10, and 100 mm, respectively.

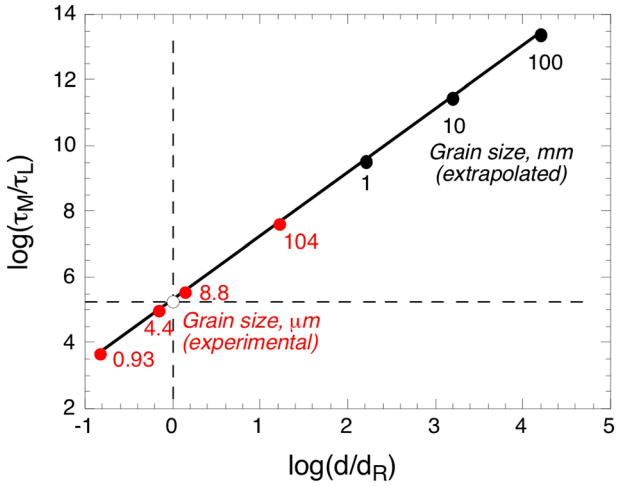

Figure 13. The linear variation of $\log(\tau_M/\tau_L)$ with $\log(d/d_R)$ for the global Burgers model (Table 2) fitted to data for MgO polycrystals 1096 and 1077, of grain sizes 4.45 and 8.8 μm, respectively.

~20% [e.g., *Irifune and Tsuchiya*, 2015]. Under these circumstances, it has been inferred from both finite element modeling [*Madi et al*., 2005] and from deformation experiments on a germanate analogue for the silicate perovskite + ferropericlase mixture [*Wang et al*., 2013] that the overall rheology should be controlled by that of the stronger, volumetrically dominant, perovskite phase. However, recent experimentation to large shear strains (~100%) on a bridgmanite + ferropericlase mixture by *Girard et al*. [2016] indicates strong partitioning of strain into the ferropericlase phase, thereby strengthening the case for shear localization in the lower mantle. Under these circumstances, the volumetrically subsidiary phase ferropericlase might have a disproportionately large influence on the mechanical properties of the lower mantle, including seismic wave dispersion and attenuation.

The extrapolation of the preferred model for the viscoelasticity of polycrystalline MgO to conditions prevailing in the uppermost lower mantle (23 GPa, and 1500°C on the mantle adiabat, and a grain size of 10 mm (Figure 12e)), suggests values of Q^{-1} increasing with increasing period across the seismic band from ~10^{-3} at 3 s to ~10^{-2} at 3000 s period. That these values are broadly comparable with the seismologically inferred dissipation of ~0.003 for the lower mantle [e.g., *Romanowicz and Mitchell*, 2015] suggests that the ferropericlase phase might be a significant contributor to seismic wave attenuation and related dispersion in the Earth's lower mantle.

For the volumetrically dominant Mg-silicate perovskite phase, the low-strain viscoelastic behavior is currently experimentally accessible only indirectly, notwithstanding pioneering forced-oscillation studies at high pressures in the D-DIA solid-medium apparatus [*Li and Weidner*, 2007]. Structural analogues for the silicate perovskites, which are stable at lower pressures, have accordingly received attention [e.g., *Webb et al*., 1999; *Harrison et al*., 2004; *Carpenter and Zhang*, 2011; *Li and Weidner*, 2012]. For the purest and microstructurally simplest of the Ca- and Sr-titanate polycrystals studied by *Webb et al*. [1999], an $SrTiO_3$ specimen of 5 μm grain size, torsional forced-oscillation tests revealed strong viscoelastic relaxation of the high-temperature background type. The dissipation Q^{-1} measured for temperatures of 900–1250°C and oscillation periods of 1–100 s was well described by a power law relationship of the form $Q^{-1} = A[T_o\exp(-E/RT)]^{\alpha}$. Similar data reported for a more impure and microstructurally more complex $CaTiO_3$ specimen of 20 μm grain size, in retrospect, provide evidence of a broad dissipation peak superimposed upon the monotonic background and moving systematically across the observational period range with increasing temperature between 1000 and 1100°C. The dissipation peak and associated dispersion of the shear modulus are reminiscent of those observed for melt-bearing olivine and impure MgO [*Webb and Jackson*, 2003]. It has been suggested that such observations may similarly reflect the stress-induced squirt of a secondary grain boundary phase of low viscosity [*Jackson*, 2015]. An indicative extrapolation to larger grain sizes was performed by *Webb et al*. [1999], but assimilation of their data for the titanate perovskites into the Burgers model, employed in this study for a comparable extrapolation to mantle conditions, awaits future work. Studies reviewed by *Carpenter and Zhang* [2011] have revealed dissipation associated with the stress-induced migration of transformational twin domain walls in various zirconate, titanate, and aluminate perovskites.

5. Conclusions

Using a multistage hot isostatic pressing procedure involving different temperatures (up to 1600°C) and different durations, high-purity, high-density specimens of polycrystalline MgO were successfully prepared

with average grain sizes ranging across more than 2 orders of magnitude (0.9–104 μm). These materials, tested in torsional forced oscillation at periods of 1–1000 s at temperatures above ~800°C, display substantial strain energy dissipation and associated modulus dispersion with well-resolved grain size sensitivity—diagnostic of the transition from elastic to viscoelastic behavior in fine-grained materials.

The observed viscoelastic relaxation is of the "high-temperature background" type and accordingly is adequately modeled by a generalized Burgers-type creep function model with a distribution $D(\tau) \sim \tau^{1-\alpha}$ of anelastic relaxation times for $\tau_L < \tau < \tau_M$ (equation (3)). The lower end (τ_L) of the anelastic absorption band is unusually well defined in dissipation data for the specimens of intermediate grain size (4.4 and 8.8 μm) by a marked decrease in $\partial \log(Q^{-1})/\partial \ln T_o$. The data constrain the exponent in the power law dependence of τ_L upon grain size to 1.1(2)—consistent with expectations (equation (1)) for elastically accommodated grain boundary sliding. Qualitatively similar observations by *Pezzotti* [1999] have been interpreted as a dissipation peak superimposed upon an otherwise more mildly period-dependent background. The upper end of the anelastic absorption band, defined by a substantial increase in $\partial \log(Q^{-1})/\partial \ln T_o$ with increasing period, which is interpreted to reflect the onset of a progressive transition toward viscous behavior, is resolved only in the highest-temperature data for the specimen of 8.8 μm grain size. Accordingly, the power law exponent describing the grain size sensitivity of the Maxwell relaxation time τ_M is fixed at 3, the value appropriate for grain boundary sliding accommodated by grain boundary diffusion (equation (2)). With the lower end of the anelastic absorption band thus plausibly associated with elastically accommodated grain boundary sliding, the upper end ascribed to the transition toward viscous behavior, and an intervening broad absorption band with mildly period-dependent dissipation, the experimental data for polycrystalline MgO are broadly compatible with expectations from the theory of grain boundary sliding as outlined in section 1.

The Burgers model fitted to the experimental data, along with an estimate of the appropriate activation volume for the viscoelastic relaxation, allows an extrapolation to the conditions of grain size, temperature, and pressure experienced by the bridgmanite + ferropericlase assemblage of the uppermost part of the Earth's lower mantle. For a grain size of 10 mm, the predicted dissipation Q^{-1} varies with increasing period from ~10^{-3} to ~10^{-2} with increasing period from 3 to 3000 s. That this range is broadly comparable with seismological observations suggests that ferropericlase might account for much of the seismic wave attenuation and associated dispersion in the lower mantle. The different grain size sensitivities of τ_L and τ_M result in a systematic broadening of the anelastic relaxation band with increasing grain size such that stresses imposed upon the lower mantle by seismic waves and tidal loading are likely to probe only the anelastic part of the mechanical response in the lower mantle.

Appendix A

The procedure pursued in Figure 10a raises an important issue concerning the nature of the additivity of background and peak contributions to the observed dissipation, and the general viability of the background subtraction performed by *Pezzotti* [1999]. For the Burgers creep function model used to fit the experimental data of the present study, the real and negative-imaginary parts of the dynamic compliance are, respectively,

$$J_1(\omega) = J_U[1 + J_{1A}(\omega)]$$

and

$$J_2(\omega) = J_U[J_{2A}(\omega) + J_{2V}(\omega)]$$

$$\text{so that } Q^{-1}(\omega) = J_2(\omega)/J_1(\omega) = [J_{2A}(\omega) + J_{2V}(\omega)]/[1 + J_{1A}(\omega)] \quad \text{(A1)}$$

[*Jackson*, 2015]. Accordingly, the dissipation prescribed by the Burgers model may be decomposed into the two additive components. The first of these, $J_{2A}(\omega)/[1 + J_{1A}(\omega)]$, represents the dissipation contributed by the anelastic absorption band, whereas the second, $J_{2V}(\omega)/[1 + J_{1A}(\omega)]$, is the extra dissipation associated with viscous relaxation. In Figure A1, such a decomposition is illustrated for the dissipation measured and modeled in the present study as a function of temperature at 101 s oscillation period for MgO polycrystal 1077 of 8.8 μm grain size. Significantly, the $\log[Q^{-1}(1/T)]$ trends for temperatures above and below the

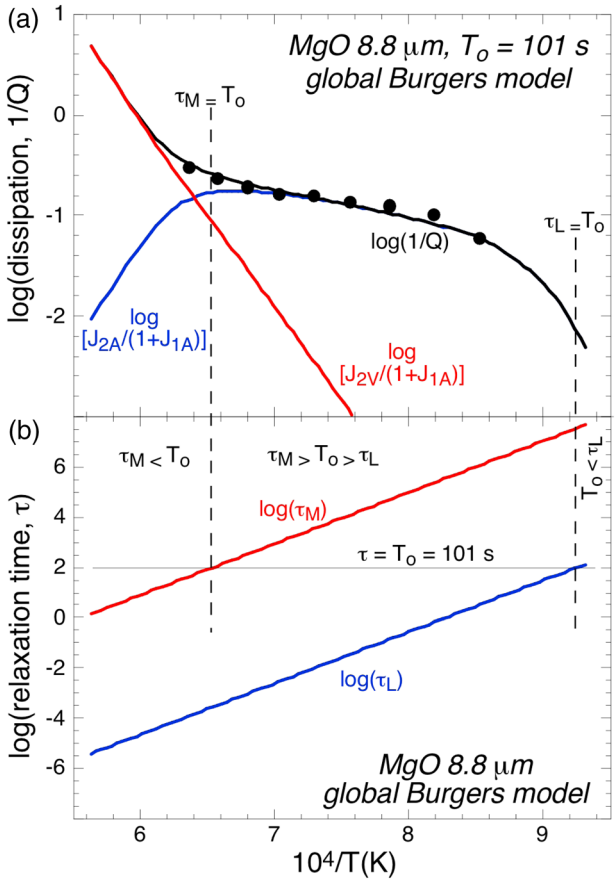

Figure A1. The relationship between the anelastic absorption band and the viscous contribution to measured/modeled dissipation: (a) The plotting symbols represent the dissipation measured in forced oscillation at 101 s period on specimen 1077 of 8.8 mm grain size, and the black, blue, and red curves denote the dissipation predicted by the global Burgers model, and its anelastic and viscous components, respectively. (b) The temperature dependence of the relaxation times τ_L and τ_M that define the lower and upper ends of the distribution of anelastic relaxation times. The intersections of the log[$\tau_i(1/T)$] trends for $i = L, M$, with the horizontal line corresponding to the oscillation period T_o = 101 s, when projected from Figure A1b into Figure A1a define the approximate extent of the anelastic absorption band.

absorption band are offset from one another rather than collinear. Thus, although the additivity of the two components is evident, it is clear that in this case the *Pezzotti* [1999] strategy for background subtraction (Figure 10a) would not be applicable.

Acknowledgments
Financial support from the Australian Research Council grant DP0450929 and technical assistance from Harri Kokkonen and Craig Saint are gratefully acknowledged. In addition, A.B. acknowledges financial support from the Netherlands Organisation for Scientific Research (NWO). The raw and processed data are available on request from the corresponding author at Ian.Jackson@anu.edu.au.

References

Anderson, O. L., and G. G. Isaak (1995), Elastic constants of mantle minerals at high temperature, in *Mineral Physics and Crystallography: A Handbook of Physical Constants*, edited by T. J. Ahrens, pp. 64–97, AGU, Washington, D. C.

Barnhoorn, A., I. Jackson, J. D. Fitz Gerald, and Y. Aizawa (2007), Suppression of elastically accommodated grain-boundary sliding in high-purity MgO, *J. Eur. Ceram. Soc.*, *27*, 4697–4703.

Carpenter, M. A., and Z. Zhang (2011), Anelasticity maps for acoustic dissipation associated with phase transitions in minerals, *Geophys. J. Int.*, *186*, 279–295.

Frost, H. J., and M. F. Ashby (1982), *Deformation-Mechanism Maps, The Plasticity and Creep of Metals and Ceramics*, Pergamon Press, Oxford, U. K.

Girard, J., G. Amulele, R. Farla, A. Mohiuddin, and S. Karato (2016), Shear deformation of bridgmanite and magnesiowüstite aggregates at lower mantle conditions, *Science*, *351*, 144–147.

Gribb, T. T., and R. F. Cooper (1998), Low-frequency shear attenuation in polycrystalline olivine: Grain boundary diffusion and the physical significance of the Andrade model for viscoelastic rheology, *J. Geophys. Res.*, *103*, 27,267–27,279, doi:10.1029/98JB02786.

Harrison, R. J., S. A. T. Redfern, and E. K. H. Salje (2004), Dynamical excitation and anelastic relaxation of ferroelastic domain walls in $LaAlO_3$, *Phys. Rev. B*, *69*, 144101.

Irifune, T., and T. Tsuchiya (2015), Phase transitions and the mineralogy of the lower mantle, in *Treatise on Geophysics*, vol. 2, 2nd ed., edited by G. Schubert, pp. 33–60, Elsevier, Amsterdam.

Itatani, K., R. Yasuda, F. Scott Howell, and A. Kishioka (1997), Effect of starting particle size on hot-pressing of magnesium oxide powder prepared by vapour-phase oxidation process, *J. Mater. Sci.*, *32*, 2977–2984.

Jackson, I. (1993), Progress in the experimental study of seismic wave attenuation, *Annu. Rev. Earth Planet. Sci.*, *21*, 375–406.
Jackson, I. (2005), Laboratory measurement of seismic wave dispersion and attenuation at high pressure and temperature, in *Advances in High-Pressure Technology for Geophysical Applications*, edited by J. Chen et al., pp. 95–119, Elsevier, Amsterdam.
Jackson, I. (2015), Properties of rocks and minerals—Physical origins of anelasticity & attenuation in rock, in *Treatise on Geophysics*, vol. 2, 2nd ed., edited by G. Schubert, pp. 539–571, Elsevier, Amsterdam.
Jackson, I., and U. H. Faul (2010), Grainsize-sensitive viscoelastic relaxation in olivine: Towards a robust laboratory-based model for seismological application, *Phys. Earth Planet. Inter.*, *183*, 151–163.
Jackson, I., and M. S. Paterson (1993), A high-pressure, high temperature apparatus for studies of seismic wave dispersion and attenuation, *Pure Appl. Geophys.*, *141*, 445–466.
Jackson, I., A. Barnhoorn, Y. Aizawa, and C. Saint (2009), Improved procedures for the laboratory study of high-temperature viscoelastic relaxation, *Phys. Earth Planet. Inter.*, *172*, 104–115.
Jackson, I., U. H. Faul, and R. Skelton (2014), Elastically accommodated grain-boundary sliding: New insights from experiment and modelling, *Phys. Earth Planet. Inter.*, *228*, 203–210.
Kampfmann, W., and H. Berckhemer (1985), High temperature experiments on the elastic and anelastic behaviour of magmatic rocks, *Phys. Earth Planet. Inter.*, *40*, 223–247.
Kê, T. S. (1947), Experimental evidence of the viscous behavior of grain boundaries in metals, *Phys. Rev.*, *71*, 533–546.
Lakki, A., R. Schaller, and C. Carry (1998), High temperature anelastic and viscoplastic deformation of fine-grained MgO-doped Al_2O_3, *Acta Mater.*, *46*, 689–700.
Lee, L. C., and S. J. S. Morris (2010), Anelasticity and grain boundary sliding, *Proc. R. Soc. A*, *466*(2121), 2651–2671.
Lee, L. C., S. J. S. Morris, and J. Wilkening (2011), Stress concentrations, diffusionally accommodated grain boundary sliding and the viscoelasticity of polycrystals, *Proc. R. Soc. A*, *467*(2130), 1624–1644.
Li, L., and D. J. Weidner (2007), Energy dissipation of materials at high pressure and high temperature, *Rev. Sci. Instrum.*, *78*, 053902, doi:10.1063/1.2735587.
Li, L., and D. J. Weidner (2012), Anelasticity and transient creep in $NaMgF_3$ perovskite at high pressure, *Phys. Earth Planet. Inter.*, *194-195*, 98–106.
Madi, K., S. Forest, P. Cordier, and M. Boussuge (2005), Numerical study of creep in two-phase aggregates with a large rheology contrast: Implications for the lower mantle, *Earth Planet. Sci. Lett.*, *237*, 223–238.
McCarthy, C., Y. Takei, and T. Hiraga (2011), Experimental study of attenuation and dispersion over a broad frequency range: 2. The universal scaling of polycrystalline materials, *J. Geophys. Res.*, *116*, B09207, doi:10.1029/2011JB008384.
Morris, S. J. S., and I. Jackson (2009), Implications of the similarity principle relating creep and attenuation in finely grained solids, *Mater. Sci. Eng. A*, *521-522*, 124–127.
Nowick, A. S., and B. S. Berry (1972), *Anelastic Relaxation in Crystalline Solids*, 677 pp., Academic Press, New York.
Pezzotti, G. (1999), Internal friction of polycrystalline ceramic oxides, *Phys. Rev. B*, *60*, 4018–4029.
Raj, R. (1975), Transient behaviour of diffusion-induced creep and creep rupture, *Metall. Trans. A*, *6A*, 1499–1509.
Raj, R., and M. F. Ashby (1972), Grain boundary sliding, and the effects of particles and its rate, *Matellurgical Trans.*, *3*, 1937–1942.
Romanowicz, B., and B. J. Mitchell (2015), Deep Earth structure—*Q* of the Earth from crust to core, in *Treatise on Geophysics*, vol. 1, 2nd ed., edited by G. Schubert, pp. 789–827, Elsevier, Amsterdam.
Takei, Y., F. Karasawa, and H. Yamauchi (2014), Temperature, grain size, and chemical controls on polycrystal anelasticity over a broad frequency range extending into the seismic range, *J. Geophys. Res. Solid Earth*, *119*, 5414–5443, doi:10.1002/2014JB011146.
Van Orman, J. A., Y. Fei, E. H. Hauri, and J. Wang (2003), Diffusion in MgO at high pressures: Constraints on deformation mechanisms and chemical transport at the core-mantle boundary, *Geophys. Res. Lett.*, *30*(2), 1056, doi:10.1029/2002GL016343.
Wang, Y., N. Hilairet, N. Nishiyama, N. Yahata, T. Tsuchiya, G. Morard, and G. Fiquet (2013), High-pressure, high-temperature deformation of $CaGeO_3$ (perovskite) ± MgO aggregates: Implications for multiphase rheology of the lower mantle, *Geochem. Geophys. Geosyst.*, *14*, 3389–3408, doi:10.1002/ggge.20200.
Webb, S., and I. Jackson (2003), Anelasticity and microcreep in polycrystalline MgO at high temperature: An exploratory study, *Phys. Chem. Miner.*, *30*, 157–166.
Webb, S., I. Jackson, and J. D. Fitz Gerald (1999), Viscoelasticity of the titanate perovskites $CaTiO_3$ and $SrTiO_3$ at high temperature, *Phys. Earth Planet. Inter.*, *115*, 259–291.